J Solid State Electrochem (2009) 13:913–919
DOI 10.1007/s10008-008-0628-x

ORIGINAL PAPER

Comparison of structure and electrochemical properties for 5 V $LiNi_{0.5}Mn_{1.5}O_4$ and $LiNi_{0.4}Cr_{0.2}Mn_{1.4}O_4$ cathode materials

Ting-Feng Yi · Chun-Yan Li · Yan-Rong Zhu · Jie Shu · Rong-Sun Zhu

Received: 5 April 2008 / Revised: 10 July 2008 / Accepted: 11 July 2008 / Published online: 30 July 2008

Abstract Spinel $LiNi_{0.5}Mn_{1.5}O_4$ and $LiMn_{1.4}Cr_{0.2}Ni_{0.4}O_4$ cathode materials have been successfully synthesized by the sol–gel method using citric acid as a chelating agent. The structure and electrochemical performance of these as-prepared powders have been characterized by X-ray diffraction (XRD), scanning electron microscopy (SEM), and the galvanostatic charge–discharge test in detail. XRD results show that there is a small $Li_yNi_{1-y}O$ impurity peak placed close to the (4 0 0) line of the spinel $LiNi_{0.5}Mn_{1.5}O_4$, and $LiMn_{1.4}Cr_{0.2}Ni_{0.4}O_4$ has high phase purity, and the powders are well crystallized. SEM indicates that $LiMn_{1.4}Cr_{0.2}Ni_{0.4}O_4$ has a slightly smaller particle size and a more regular morphological structure with narrow size distribution than those of $LiNi_{0.5}Mn_{1.5}O_4$. Galvanostatic charge–discharge testing indicates that the initial discharge capacities of $LiMn_{1.4}Cr_{0.2}Ni_{0.4}O_4$ and $LiNi_{0.5}Mn_{1.5}O_4$ cycled at 0.15 C are 129.6 and 130.2 mAh g^{-1}, respectively, and the capacity losses compared to the initial value, after 50 cycles, are 2.09% and 5.68%, respectively. $LiMn_{1.4}Cr_{0.2}Ni_{0.4}O_4$ cathode has a higher electrode coulombic efficiency than that of the $LiNi_{0.5}Mn_{1.5}O_4$ cathode, implying that Ni and Cr dual substitution is beneficial to the reversible intercalation and de-intercalation of Li^+.

Keywords Lithium ion battery · Cathode material · $LiMn_{1.4}Cr_{0.2}Ni_{0.4}O_4$ · $LiNi_{0.5}Mn_{1.5}O_4$ · Electrochemical property

Introduction

Lithium ion batteries are regarded as promising new power sources for hybrid electric vehicles as well as for portable electronic devices due to their long cycle life and high energy density. Their most promising cathodes are olivine-type $LiFePO_4$ and spinel $LiMn_{2-x}M_xO_4$ (M—transition metal or Mg, Al, etc.) because of their low material cost, high natural abundance, environmental harmlessness, and good safety compared with the $LiCoO_2$ used in current batteries [1–20]. While $LiFePO_4$ has been demonstrated to have high reversible capacity and intrinsic safety, thanks to its electrochemically stable phosphate group [1, 2], $LiMn_{2-x}M_xO_4$ is a better choice in high-power applications due to its much higher average discharge potential, especially when doped with transition metals. On the other hand, spinel $LiMn_2O_4$ has a higher potential (4 V vs. Li/Li^+) and a higher material density (4.2 g cm^{-3}) than those of $LiFePO_4$ (3.45 V vs. Li/Li^+ and 3.6 g cm^{-13}, respectively). In addition, $LiFePO_4$ also suffers from very low electronic conductivity. Transition metal oxide spinels possess rich crystal chemistries due to the ability of transition metals to adopt different valence states. This can be induced by changing the starting composition, annealing temperature,

T.-F. Yi (✉) · Y.-R. Zhu · R.-S. Zhu
School of Chemistry and Chemical Engineering,
Anhui University of Technology,
No 59 Hudong Road,
Maanshan 243002, People's Republic of China
e-mail: tfyihit@163.com

C.-Y. Li
Department of Pharmacy, Mudanjiang Medical University,
Mudanjiang,
Heilongjiang 157011, People's Republic of China

J. Shu (✉)
Energy Technology Research Institute, National Institute
of Advanced Industrial Science and Technology (AIST),
Umezono 1-1-1,
Tsukuba, Ibaraki 305-8568, Japan
e-mail: sjshujie@126.com

or atmosphere, i.e. oxidizing or reducing. Among $LiMn_{2-x}M_xO_4$ (M = transition metal) materials, $LiMn_{1.5}Ni_{0.5}O_4$ shows good cycling stability on repeated lithium ion extraction and insertion, making it the most attractive material for practical application [8, 9]. $LiNi_{0.5}Mn_{1.5}O_4$ shows not only high oxidation voltage but also higher stability than layered lithium cobalt nickel oxide [10]. However, it has been reported that $LiNi_{0.5}Mn_{1.5}O_4$ synthesized at above 650 °C loses oxygen and disproportionates to a spinel with a smaller Ni content and $Li_yNi_{1-y}O$, which leads to a decrease in the nickel content in the spinel phase and a consequent introduction of some Mn^{3+}. This is closely related to the oxygen deficiency during the processing[11]. The presence of Mn^{3+} in $LiNi_{0.5}Mn_{1.5}O_4$ causes the development of a 4-V plateau and a decrease in 5-V capacity. In addition, Lee et al. [12] have also reported that the solubility limit of Ni in the $LiNi_xMn_{2-x}O_4$ system is 0.415. It has been reported that Cr^{3+} ions have high oxygen affinity, providing structural stability during cycling [13, 14]. So far, many chemical routes have been used to synthesize spinel $LiNi_{0.5}Mn_{1.5}O_4$ powders. These synthesis methods include solid-state reaction [15], sol–gel [16], emulsion drying [17], carbonate processing [18], and molten salt processes [19], etc. A sol–gel process has been used for the synthesis to obtain homogeneity and narrow particle size distribution of the final $LiNi_{0.5}Mn_{1.5}O_4$ product, and it has been widely used to prepare cathode materials for lithium ion batteries [16, 20]. Wu et al. [21] have reported that the substitution of chromium ions in $LiMn_{2-x}Cr_xO_4$ results in a conversion of Cr^{3+} to Cr^{6+} for $x>0.2$ and in the formation of $LiCrO_2$ impurity for $x>0.8$. In this article, the spinels $LiMn_{1.4}Cr_{0.2}Ni_{0.4}O_4$ and $LiNi_{0.5}Mn_{1.5}O_4$ were synthesized by the sol–gel method, and their structures and electrochemical behavior were investigated. It provides not only an effective route of synthesis but also a way to modify Li–Mn–O spinel as a promising cathode material.

Experimental

Preparation of materials

The samples of $LiNi_{0.5}Mn_{1.5}O_4$ and $LiMn_{1.4}Cr_{0.2}Ni_{0.4}O_4$ spinel were prepared by a sol–gel method using citric acid as a chelating agent. Stoichiometric amounts of Li $(CH_3COO)\cdot 2H_2O$(AR, 99%), $Mn(CH_3COO)_2\cdot 6H_2O$(AR, 99%), $Ni(NO_3)_2\cdot 6H_2O$(AR, 99%) and $Cr(NO_3)_3\cdot 9H_2O$ (AR, 99%) were separately dissolved in citric acid solution with continuous stirring, and the molar ratio of citric acid to total metal cations was fixed at 1:1. The pH of the mixed solution was adjusted to 7 by adding $NH_3\cdot H_2O$ (AR, 25%). The mixed solution was then heated with continuous stirring up to boiling point until a gel was obtained. The gel was dried at about 110 °C for 12 h in a vacuum drying oven, resulting in the formation of amorphous powders. The powder was again dried at 850 °C for 20 h in air to obtain the final spinel product.

Physical characterization of materials

Powder X-ray diffraction (XRD) was performed using a Rigaku D/MAX-RC X-ray diffractometer (Hitachi, Japan) with Cu $K\alpha_1$ (45 kV, 50 mA, step size=0.02°, $10°<2\theta<90°$) monochromated radiation to identify the crystalline phase of the materials. The particle morphologies of the samples were examined using a scanning electron microscope (Hitachi, S-4000 and S-570).

Electrochemical performance of materials

Charge–discharge performance of the cell was characterized galvanostatically on Land 2000T (Wuhan, China) tester at 0.15 C charge–discharge rate between 3.5 and 4.98 V (vs. Li/Li^+). The upper limit was set at 4.98 V to prevent increasing the charge capacity by effect of side reactions such as release of oxygen from the spinel lattice above 5.0 V.

Preparation of lithium ion batteries

The coin cell cathode paste was prepared by mixing 85 wt.% of active material with 5 wt.% of polyvinylidene fluoride and 10 wt.% of acetylene black in *N*-methyl-2-pyrrolidinone and, subsequently, a slurry was made. The mixed slurry was coated onto an aluminum current collector and vacuum-dried at 110 °C overnight before use. Coin cells were prepared in a dry argon atmosphere inside a glove box. The cathode and Li anode were separated inside the coin cell using Celgard 2300 membrane. Commercial $LiPF_6$ (1 M) in a 1:1 (by volume) mixture of ethylene carbonate and dimethyl carbonate was used as electrolyte.

Results and discussion

Micrographs and structure analysis

Figure 1 shows the XRD patterns of as-prepared $LiNi_{0.5}Mn_{1.5}O_4$ and $LiMn_{1.4}Cr_{0.2}Ni_{0.4}O_4$ powders. All the peak signatures of the XRD pattern for $LiNi_{0.5}Mn_{1.5}O_4$ and $LiMn_{1.4}Cr_{0.2}Ni_{0.4}O_4$ conform to JCPDS card No-35-782, suggesting that they are both single-phase spinel compounds. The sharp peaks in the patterns show good crystallinity of the cathodes. In addition to the spinel reflections, the pattern shows a few weak reflections corresponding to the impurity phase $Li_xNi_{1-x}O$ having the

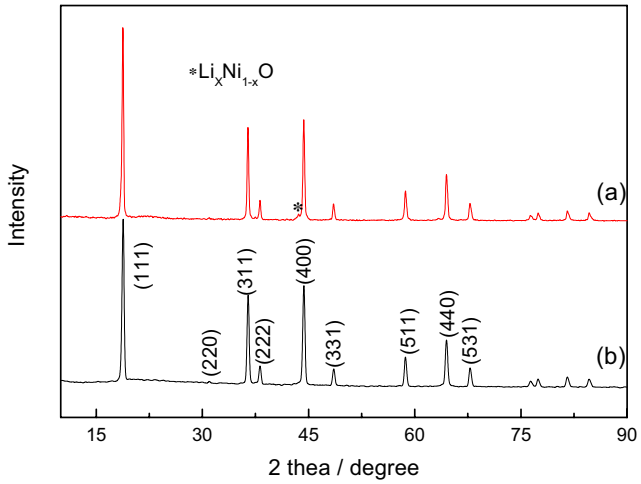

Fig. 1 Typical XRD patterns for the samples: **a** $LiNi_{0.5}Mn_{1.5}O_4$; **b** $LiMn_{1.4}Cr_{0.2}Ni_{0.4}O_4$

rock salt structure, as is observed in Fig. 1a, which is in agreement with previous reports [11], indicating that Ni substitution alone did not help to form a pure spinel structure. The reflections marked with (*h*, *k*, *l*) values refer to the spinel phase, and those marked with (*) refer to the impurity phase $Li_yNi_{1-y}O$. The formation of the $Li_yNi_{1-y}O$ impurity phase results in a decrease in Ni content and Mn valence in the spinel phase as shown by the generalized reaction:

$$LiMn_{1.5}Ni_{0.5}O_4 \rightarrow \alpha Li_yNi_{1-y}O + \beta LiMn_{1.5+x}Ni_{0.5-x}O_4 + \gamma O_2 \quad (1)$$

where α, β, and γ define, respectively, the relative amounts of the $Li_yNi_{1-y}O$, $LiNi_{0.5-x}Mn_{1.5+x}O_4$, and O_2 phases. This observation suggests that the solubility limit of Ni in the $LiMn_{2-x}Ni_xO_4$ spinel phase may be $x<0.5$, which is in agreement with the previous reports [12]. The integration of the XRD pattern shows that the content of $Li_yNi_{1-y}O$ is approximately 1% of the total spinel phase, from the peak area comparison in the diffractograms. $LiMn_{1.4}Cr_{0.2}Ni_{0.4}O_4$ materials are confirmed as a cubic spinel structure with a space group of *Fd*3*m* in which lithium ions occupy the tetrahedral (8a) sites, transition metals (Ni, Cr and Mn) are located at the octahedral (16d) sites, and oxygen atoms reside in the 32e sites, as shown in Fig. 1b. This indicates that the Mn site in $LiMn_2O_4$ can be fully substituted by Ni and Cr. The results show that the Cr doped $LiMn_{1.4}Cr_{0.2}Ni_{0.4}O_4$ contains more oxygen than that of undoped $LiNi_{0.5}Mn_{1.5}O_4$, implying that Cr plays a crucial role in the maintenance of the oxygen in the cathode. The lattice parameters and unit cell volumes of these compounds are listed in Table 1. The lattice parameters were calculated through the least square program method from the diffraction data of $LiNi_{0.5}Mn_{1.5}O_4$ and $LiMn_{1.4}Cr_{0.2}Ni_{0.4}O_4$ and were found to be about 8.174 and 8.169 Å, respectively, which is slightly less than that of a pure $LiMn_2O_4$ cathode material [8.24762(16) Å (35-0782 JCPDS file)]. This prevents a phase transition of the material. However, $LiMn_{1.4}Cr_{0.2}Ni_{0.4}O_4$ has a smaller lattice parameter than that of $LiNi_{0.5}Mn_{1.5}O_4$. This may be explained by the fact that: (1) the ionic radius of Cr^{3+} ion (0.615 Å) is smaller than those of Mn^{3+}(0.66 Å) and Ni (0.69 Å)[22], leading to the shrinkage of the spinel framework; (2) the bonding energy of Cr–O (427 kJ mol^{-1}) is stronger than that of Mn–O (402 kJ mol^{-1}) and Ni–O (391.6 kJ mol^{-1}), revealing that the former has a higher octahedral site preference energies [22, 23], which results in the diminution of the bond length. The stronger Cr–O bond can also stabilize the spinel structure by assisting retention of the local symmetry during cycling.

In a spinel-framework structure having space group symmetry of *Fd*3*m*, the mean bond length of cations (*R*) is given by the following equations:

$$R_{Mn-Mn(Ni,Cr)} = \frac{\sqrt{2}}{4}a \quad (2)$$

$$R_{Mn(Ni,Cr)-O} = a\sqrt{3u^2 - 2u + 0.375} \quad (3)$$

where *a* is the lattice parameter of the spinel phase, and *u* is the oxygen positional parameter (*u*, 0.267) [24]. The calculated results are recorded in Table 1. The results show that the substitution of Cr shortens the mean bond length of cations, increases the mean bond energy, and improves structural stability. This means that the Cr-doped $LiMn_{1.4}Cr_{0.2}Ni_{0.4}O_4$ may have excellent electrochemical cycle stability. Ohzuku et al. [25] have reported that any occupancy of the substituent ions in the 8*a* tetrahedral lithium sites will lead to unfavorable electrochemical characteristics. According to Ohzuku et al. [25], the integrated intensity ratios of the (4 0 0)/(3 1 1) and (2 2 0)/(3 1 1) peaks are indices of the extent of occupancy of the

Table 1 Structural parameters of $LiNi_{0.5}Mn_{1.5}O_4$ and $LiMn_{1.4}Cr_{0.2}Ni_{0.4}O_4$

Sample	Lattice parameter (Å)	Unit cell volume (Å^3)	$R_{Mn-Mn(Cr,\ Ni)}$ (Å)	$R_{Mn(Cr,\ Ni)-O}$ (Å)
$LiNi_{0.5}Mn_{1.5}O_4$	8.174	546.1	2.890	1.915
$LiMn_{1.4}Cr_{0.2}Ni_{0.4}O_4$	8.169	545.1	2.888	1.913

substituent ions in the 8*a* lithium sites. There is an obscure (2 2 0) peak (at $2\theta \approx 31°$) in $LiMn_{1.4}Cr_{0.2}Ni_{0.4}O_4$ as shown in Fig. 1, which is associated with the presence of heavy cations in tetrahedral 8*a* sites of the spinel-type structure. However, in the $LiMn_{1.4}Cr_{0.2}Ni_{0.4}O_4$ samples, the integrated intensity ratio of the (4 0 0)/(3 1 1) increases compared to $LiNi_{0.5}Mn_{1.5}O_4$. This suggests that nickel shows a propensity to occupy the 8*a* lithium sites in $LiNi_{0.5}Mn_{1.5}O_4$ due to the $Li_yNi_{1-y}O$ impurity.

Figure 2 shows the scanning electron microscopy (SEM) image of these materials. $LiMn_{1.4}Cr_{0.2}Ni_{0.4}O_4$ powders have a uniform, nearly cubic structural morphology with narrow size distribution under 1 μm. These can be attributed to the action of the chelating agent citric acid, which forms a complex network where the metal ions are uniformly distributed in the matrix. Thus, it prevents phase separation and leads to the formation of homogeneous sized particles during thermal decomposition. However, $LiNi_{0.5}Mn_{1.5}O_4$ powders have a wide particle size distribution ranging from 1 to 5 μm. The result suggests that Cr ions are successively substituted for Mn in the $LiMn_{1.4}Cr_{0.2}Ni_{0.4}O_4$ host structure, resulting in sufficient contact between active materials and electrolyte and resulting in favorable diffusion and transmission of Li^+ in the electrode.

Electrochemical performance analysis

Figure 3 shows the room temperature charge–discharge characteristics of coin cells carried out galvanostatically between 3.5- and 4.98-V cutoff limits, and Table 2 lists the first discharge capacities obtained in different voltage regions. From the charge–discharge curves, it can be seen that $LiMn_{1.4}Cr_{0.2}Ni_{0.4}O_4$ exhibits three potential plateaus, but $LiNi_{0.5}Mn_{1.5}O_4$ shows only two potential plateaus. One is around the 4.1-V range, which corresponds to the redox reaction involving Mn^{3+}/Mn^{4+}. The other plateaus are observed in the 4.7- and 4.8-V potential regions. These two plateaus correspond to the redox reactions involving Ni^{2+}/Ni^{4+} and Cr^{3+}/Cr^{4+}, respectively. The delithiation (charge)/lithiation (discharge) reactions into/from spinel

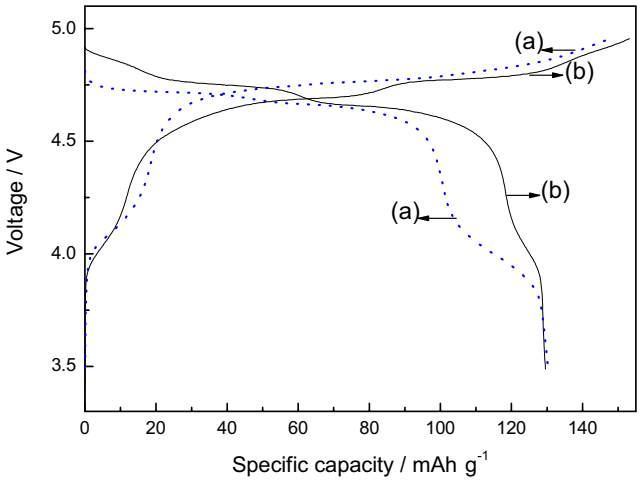

Fig. 3 First discharge profiles of $LiNi_{0.5}Mn_{1.5}O_4$ (**a**) and $LiMn_{1.4}Cr_{0.2}Ni_{0.4}O_4$ (**b**) series of spinel oxides, recorded at 0.15 C discharge rate between 4.98 and 3.5 V

$LiMn_2O_4$, $LiNi_{0.5}Mn_{1.5}O_4$ and $LiMn_{1.4}Cr_{0.2}Ni_{0.4}O_4$ proceed reversibly according to the following equations:

$$Li^+Mn^{3+}Mn^{4+}O_4 \rightleftharpoons Mn_2^{4+}O_4 + Li^+ + e^- \quad (4)$$

$$Li^+Mn_{1.5}^{4+}Ni_{0.5}^{2+}O_4 \rightleftharpoons Mn_{1.5}^{4+}Ni_{0.5}^{4+}O_4 + Li^+ + e^- \quad (5)$$

$$LiMn_{1.4}^{4+}Cr_{0.2}^{3+}Ni_{0.4}^{2+}O_4 \rightleftharpoons Mn_{1.4}^{4+}Cr_{0.2}^{4+}Ni_{0.4}^{4+}O_4 + Li^+ + e^- \quad (6)$$

As shown by these equations, the charge–discharge reactions may be classified into three processes: Eq. 4 corresponding to Mn^{3+}/Mn^{4+}, Eq. 5 corresponding to Ni^{2+}/Ni^{4+}, and Eq. 6 corresponding to Ni^{2+}/Ni^{4+} and Cr^{3+}/Cr^{4+}, respectively. The initial capacities of $LiNi_{0.5}Mn_{1.5}O_4$ and $LiMn_{1.4}Cr_{0.2}Ni_{0.4}O_4$ are 130.2 and 129.6 mAh g^{-1}, respectively. It is clear that both samples have nearly equal initial capacities, but $LiMn_{1.4}Cr_{0.2}Ni_{0.4}O_4$ has a higher discharge potential plateau than that of $LiNi_{0.5}Mn_{1.5}O_4$. In addition, $LiMn_{1.4}Cr_{0.2}Ni_{0.4}O_4$ has higher discharge capacity (at

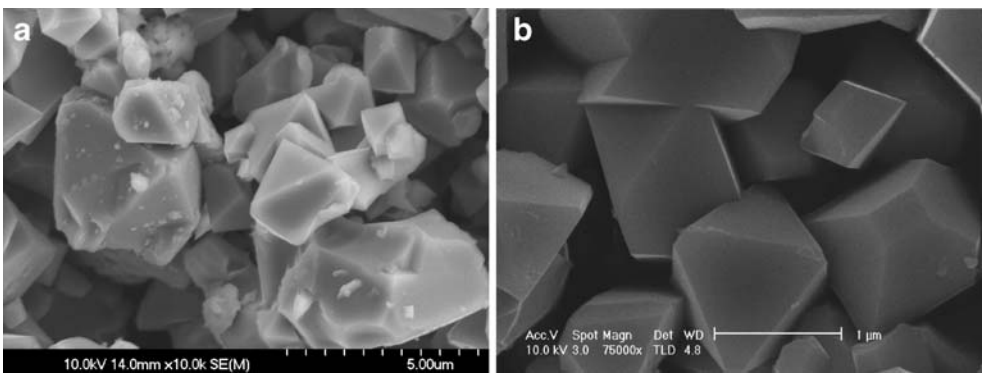

Fig. 2 SEM pictures of $LiNi_{0.5}Mn_{1.5}O_4$ (**a**) and $LiMn_{1.4}Cr_{0.2}Ni_{0.4}O_4$ (**b**)

Table 2 Cycle performance data of the prepared powders for the first cycle and the 50th cycle

Samples	Initial discharge capacity ($mAh \cdot g^{-1}$)	Initial discharge capacity at 5–4.1 V ($mAh \cdot g^{-1}$)	Initial discharge capacity at 4.1–3.5 V ($mAh \cdot g^{-1}$)	Discharge capacity after 50 cycles ($mAh \cdot g^{-1}$)	Capacity loss (%)
$LiNi_{0.5}Mn_{1.5}O_4$	130.2	106.9	23.3	122.8	5.68
$LiMn_{1.4}Cr_{0.2}Ni_{0.4}O_4$	129.6	120.5	9.1	126.9	2.09

5–4.1 V) than that of $LiNi_{0.5}Mn_{1.5}O_4$, so that the former has a better electrochemical performance than the latter, and it also indicates that the latter has a higher content of Mn^{3+} ions. The atomic radius of Mn^{4+} ion is smaller than that of Mn^{3+} ion, which means that $LiMn_{1.4}Cr_{0.2}Ni_{0.4}O_4$ has a smaller lattice parameter than that of $LiNi_{0.5}Mn_{1.5}O_4$ because the latter contains more Mn^{3+} ion than the former, which is consistent with the XRD results in Table 1. This prevents the phase transition of the spinel material. The differences in Mn^{3+} ion content between $LiNi_{0.5}Mn_{1.5}O_4$ and $LiMn_{1.4}Cr_{0.2}Ni_{0.4}O_4$ materials may be due to the high chemical affinity of Cr for oxygen [26], which provides excess capacity in the 4.8-V region, stable intercalation in the high voltage range.

Figure 4 shows typical galvanostatic charge–discharge cycling performance curves for electrodes cycled at 0.15 C made from prepared powders. Table 2 summarizes their cycling performance. The capacity loss was calculated after the first 50 cycles, which is defined as $(C_1-C_n)/C_1\times 100\%$, where C_1 and C_n are the discharge capacities of the first and nth cycle, and n is the number of cycles. It is found that both samples have better cycling performance, as shown in Fig. 4, which is related to the presence of the dopant ions. This may be explained that the Jahn–Teller distortion is effectively constrained by the substitution of Ni^{2+} and Cr^{3+} for Mn^{3+} ions. $LiMn_{1.4}Cr_{0.2}Ni_{0.4}O_4$ has a larger discharge capacity after two cycles and much lower capacity loss rate after 50 cycles than those of $LiNi_{0.5}Mn_{1.5}O_4$, as is shown in Table 2. The reason for this may be as follows. It has been reported that HF generated during cycling when using $LiPF_6$-based electrolyte was responsible for the dissolution of manganese [27]. In addition, Mn^{3+} is considered to be the main source of the dissolution of manganese via Hunter's reaction [28]:

$$4H^+ + 2LiMn^{3+}Mn^{4+}O_4 \rightarrow 3(\lambda-MnO_2)+Mn^{2+}+2Li^+ + 2H_2O \quad (7)$$

The protonated λ-MnO_2 cannot act as a host for lithium ions during cycling because of the strong binding energy of the protons to the oxygen sites around the 16*d* Mn [29]. Furthermore, F^- can also trap soluble Mn^{2+} and lead to the precipitation of MnF_2. At the same time, the deliquescent manganese fluoride deposits on the surface of negative electrode on which the passivation layer forms. This reduces conductance and blocks the transport of electrons or ions [30], reducing the electrochemical performance of $LiNi_{0.5}Mn_{1.5}O_4$. According to the analysis in Fig. 3, doping with Ni and Cr ions reduces the Mn^{3+} content in $LiMn_{1.4}Cr_{0.2}Ni_{0.4}O_4$, slowing the dissolution of Mn^{3+} ions and thereby increasing cycling performance. Furthermore,

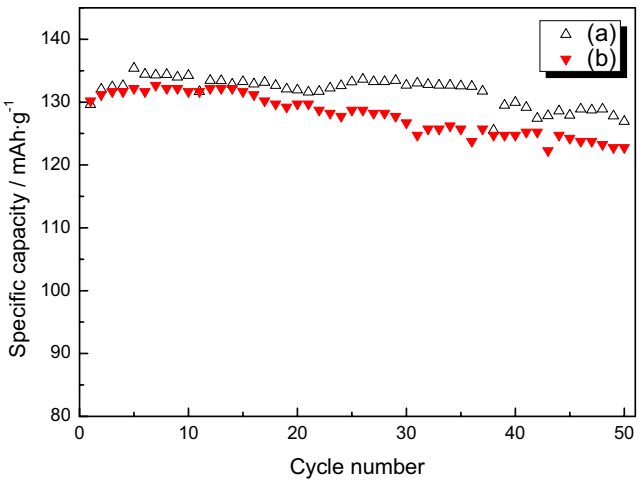

Fig. 4 Cycling performance of different cathode materials: **a** $LiMn_{1.4}Cr_{0.2}Ni_{0.4}O_4$ and **b** $LiNi_{0.5}Mn_{1.5}O_4$

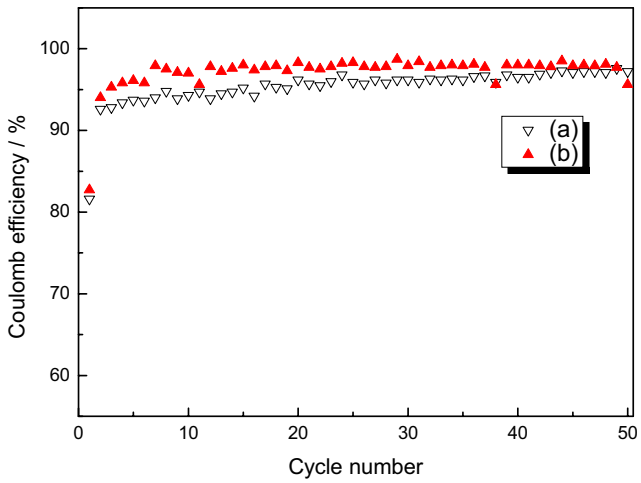

Fig. 5 Coulombic efficiency of $LiNi_{0.5}Mn_{1.5}O_4$ (**a**) and $LiMn_{1.4}Cr_{0.2}Ni_{0.4}O_4$ (**b**) in 50 cycles

better crystallinity and more regular morphology of $LiMn_{1.4}Cr_{0.2}Ni_{0.4}O_4$ powders would help to release the stresses generated by the repetitive Li^+ intercalation; smaller particles (see Fig. 2b) can provide more interfacial area for contact within the liquid electrolyte and hence can increase the opportunity for lithium ions to intercalate into the host structure [31]. These are consistent with the XRD and SEM results discussed above; moreover, $LiMn_{1.4}Cr_{0.2}Ni_{0.4}O_4$ has a higher theoretical capacity than that of $LiMn_{1.5}Ni_{0.5}O_4$ due to the low molecular weight of Cr compared with that of Ni [32].

To study the influence of the dopant ions on the electrochemical behavior of spinel lithium manganese oxide, the result of the coulomb efficiency of both electrodes is plotted in Fig. 5. This efficiency is defined as the discharge capacity divided by the charge capacity in one charge/discharge cycle. It is interesting that the coulombic efficiencies of both electrodes in the first charge–discharge cycle are less than 85%, indicating that a small fraction of lithium ions is incapable of intercalating back into the host structure due to electrolyte decomposition at high voltage. However, after about two cycles, the coulomb efficiencies of both electrodes are increased to nearly a constant value (more than 90%). The improved cycling efficiency of the samples after the first charge–discharge process may be attributed to the formation of protective layer on the electrode surface. It is obvious that the $LiMn_{1.4}Cr_{0.2}Ni_{0.4}O_4$ electrode has a higher mean coulombic efficiency than that of the $LiNi_{0.5}Mn_{1.5}O_4$ electrode. This result implies that Ni and Cr dual substitution is beneficial to the reversible intercalation and de-intercalation of Li^+. It also shows that the $LiMn_{1.4}Cr_{0.2}Ni_{0.4}O_4$ material has a better electrochemical performance than $LiNi_{0.5}Mn_{1.5}O_4$, which may be related to its better crystallinity and more regular morphology. The features of $LiMn_{1.4}Cr_{0.2}Ni_{0.4}O_4$ examined here are very desirable for its use as a cathode to improve the electrochemical properties of lithium ion batteries.

Conclusions

$LiNi_{0.5}Mn_{1.5}O_4$ and $LiMn_{1.4}Cr_{0.2}Ni_{0.4}O_4$ cathode materials were successfully synthesized by sol–gel method. The $I(400)/I(311)$ratio as well as the lattice parameter and smaller particle size of $LiMn_{1.4}Cr_{0.2}Ni_{0.4}O_4$ are expected to show better electrochemical performance than that of $LiMn_{1.5}Ni_{0.5}O_4$. $LiMn_{1.4}Cr_{0.2}Ni_{0.4}O_4$ has a uniform and narrow size distribution under 1 μm. The substitutions of a small amount of Cr^{3+} simultaneously for both Mn^{4+} and Ni^{2+} to give $LiMn_{1.4}Cr_{0.2}Ni_{0.4}O_4$ are found to suppress the 4-V plateau and increase the 5-V capacity. $LiMn_{1.4}Cr_{0.2}Ni_{0.4}O_4$ shows a better combination of high 5-V capacity (120.5 mAh g^{-1} at 5–4.1 V), excellent capacity retention (97.91% in 50 cycles), and coulombic efficiency. The excellent performance of $LiMn_{1.4}Cr_{0.2}Ni_{0.4}O_4$ coupled with its low cost may make it attractive for high-power applications such as electric and hybrid vehicles.

Acknowledgments The authors thank Prof. Xinguo Hu of Harbin Institute of Technology and Dr. Ying Wang of Institute of Chemistry, Chinese Academy of Sciences for their helpful discussion on the experimental techniques.

References

1. Padhi AK, Nanjundaswamy KS, Goodenough JB (1997) J Electrochem Soc 144:1188 doi:10.1149/1.1837571
2. Takahashi M, Tobishima S, Takei K, Sakurai Y (2002) Solid State Ionics 148:283 doi:10.1016/S0167-2738(02)00064-4
3. Yi TF, Hu XG, Gao K (2006) J Power Sources 162:636 doi:10.1016/j.jpowsour.2006.07.019
4. Dokko K, Anzue N, Mohamedi M, Itoh T, Uchida I (2004) Electrochem Commun 6:384 doi:10.1016/j.elecom.2004.02.005
5. Zeng RH, Li WS, Lu DS, Huang QM (2007) J Power Sources 174:592 doi:10.1016/j.jpowsour.2007.06.120
6. Yi TF, Zhu YR (2008) Electrochim Acta 53:3120 doi:10.1016/j.electacta.2007.11.062
7. Taniguchi I, Bakenov Z (2005) Powder Technol 159:55 doi:10.1016/j.powtec.2005.07.002
8. Xu HY, Xie S, Ding N, Liu BL, Shang Y, Chen CH (2006) Electrochim Acta 51:4352 doi:10.1016/j.electacta.2005.12.014
9. Aurbach D, Markovsky B, Talyossef Y, Salitra G, Kim H-J, Choi S (2006) J Power Sources 162:780 doi:10.1016/j.jpowsour.2005.07.009
10. Patoux S, Sannier L, Lignier H, Reynier Y, Bourbon C, Jouanneau S et al (2008) Electrochim Acta 53:4137 doi:10.1016/j.electacta.2007.12.054
11. Zhong Q, Bonakdarpour A, Zhong M, Gao Y, Dahn JR (1997) J Electrochem Soc 144:205 doi:10.1149/1.1837386
12. Lee YS, Todorov YM, Konishi T, Yoshio M (2001) ITE Lett 1:1 doi:10.1086/324437
13. Robertson AD, Howard WF Jr (1997) J Electrochem Soc 144:3505 doi:10.1149/1.1838041
14. Sigala C, Verbaere A, Mansot JL, Guyomard D, Piffard Y, Tournoux M (1997) J Solid State Chem 132:372 doi:10.1006/jssc.1997.7476
15. Fang H-S, Wang Z-X, Li X-H, Guo H-J, Peng W-J (2006) J Power Sources 153:174 doi:10.1016/j.jpowsour.2005.03.179
16. Xu HY, Xie S, Ding N, Liu BL, Shang Y, Chen CH (2006) Electrochim Acta 51:4352 doi:10.1016/j.electacta.2005.12.014
17. Myung S-T, Komaba S, Kumagai N, Yashiro H, Chung H-T, Cho T-H (2002) Electrochim Acta 47:2543 doi:10.1016/S0013-4686(02)00131-7
18. Lee YS, Sun YK, Ota S, Miyashita T, Yoshio M (2002) Electrochem Commun 4:989 doi:10.1016/S1388-2481(02)00491-5
19. Kim J-H, Myung S-T, Sun Y-K (2004) Electrochim Acta 49:219 doi:10.1016/j.electacta.2003.07.003
20. Yi TF, Dai CS, Gao K, Hu XG (2006) J Alloy Compd 425:343 doi:10.1016/j.jallcom.2006.01.054
21. Wu C, Wu F, Chen L, Huang X (2002) Solid State Ionics 152-153:335 doi:10.1016/S0167-2738(02)00328-4
22. Yi TF, Hu XG, Huo HB, Gao K (2006) Rare Met Mat Eng 35:1350
23. Dean JA (1992) Lange's handbook of chemistry, 4th edn. McGraw-Hill, New York, pp 4.12–4.38

24. Ohzuku T, Takeda S, Iwanaga M (1999) J Power Sources 81-82:90 doi:10.1016/S0378-7753(99)00246-3
25. Ohzuku T, Ariyoshi K, Takeda S, Sakai Y (2001) Electrochim Acta 46:2327 doi:10.1016/S0013-4686(00)00725-8
26. Hosoya M, Ikuta H, Wakihaha M (1998) Solid State Ionics 111:153 doi:10.1016/S0167-2738(98)00156-8
27. Jang DH, Shin YJ, Oh SM (1996) J Electrochem Soc 143:2204 doi:10.1149/1.1836981
28. Hunter JC (1981) J Solid State Chem 39:142 doi:10.1016/0022-4596(81)90323-6
29. Pasquier AD, Blyr A, Courjal P, Larcher D, Amatucci G, Gerand B et al (1999) J Electrochem Soc 146:428 doi:10.1149/1.1391625
30. Tarascon JM, Mckinnon WR, Coowar F, Bowmer TN, Amatucci G, Guyomard D (1994) J Electrochem Soc 141:1421 doi:10.1149/1.2054941
31. Yi TF, Hu XG (2007) J Power Sources 167:185 doi:10.1016/j.jpowsour.2007.02.003
32. Hong K-J, Sun Y-K (2002) J Power Sources 109:427 doi:10.1016/S0378-7753(02)00101-5